Nanosecond Time Resolution: Technical, Implementation and Usefulness

J. Verdebout and C. Koechler

Commission of the European Communities - Joint Research Center
Institute for Remote Sensing Applications 21020 Ispra (Varese), Italy

ABSTRACT

This paper reports on laboratory lidar measurements with a high temporal resolution performed on samples of crude oils and on an artificial water column. It shows how this technique can help in identifying the oil type and assesses its possibilities in measuring the water attenuation characteristics. It then describes a flight instrument, the "Time Resolved Lidar Fluorosensor" (TRLF) designed to implement this type of measurements from an aircraft. The basic capability of the TRLF is to perform spectro-temporal measurements of the lidar signals with a time resolution of 1 ns and spectral resolution of 15 nm (range from 350 to 710 nm).

INTRODUCTION

In the panel of instruments used for monitoring the oil pollution at sea, the lidar fluorosensors are the instruments which can give an information on the nature of the product present in a slick. It has been shown that the laser induced fluorescence spectrum allows to distinguish between refined products such as diesel fuels, crude oils and heavy residuals, the emission maximum being found more towards the short wavelengths for the lighter products (O'Neil et al.,1980). The same trend exists in the emission spectra of the various crude oils but to a smaller extent and it is generally recognized that the crude oil type identification is difficult with a classical lidar working with a few spectral channels. In order to increase the instrument discriminating power, one can use high spectral resolution, multiple wavelength excitation (Dudelzak et al., 1991) or time resolution. The crude oils have indeed a large range of fluorescence time decay with characteristic time constants from 0.4 ns (heavier ones) to 18 ns (lighter ones). Besides, the characterization of an oil slick at sea is further complicated by weathering processes such as the separation into fractions, evaporation, emulsification (Diebel-Langohretal.,1985);here too an increased discriminating power of the instrument is desirable. Time resolution also gives access to the depth dependence of the signal and should therefore be useful to locate subsurface oil and to distinguish the fluorescence of an oil film from the contribution of the Dissolved Organic Matter (DOM). This last problem is particularly acute for film thickness measurements (Visser,1979; Burlamacchi et al.,1983; Hoge,1983; Barbini et al., 1990; Hengstermann and Reuter, 1990).

Depth resolution should also prove itself valuable for oceanographic applications. The various water column signals intensity is indeed largely affected by the optical properties of water (Brisow et al.,1981; Exton et al.,1983; Poole and Esaias,1983; Dittman and Hallett,1988). Within certain limits, the time resolution allows the direct measurement of the water attenuation coefficient and consequently the introduction of this important parameter in the analysis.

However, it has been evaluated that, to be useful, the time resolution should be at least 1 ns and that the instrument should retain spectral resolution (Diebel et al.,1987). Besides, the laser beam diameter should be snlall in order to minimize the perturbing effects of the waves and of multiple scattering on the signals time dependence. This paper presents the instrument built to meet these requirements. It also reports measurements on oil samples and on an artificial water column, performed in the JRC simulation laboratory.

1. LABORATORY INSTRUMENTATION

Figure 1 shows the experimental setup for a simulation experiment on an artificial water column. The excitation source is a commercial mode-locked Nd- YAG laser (Quantel YG 503 20) from which the second and third harmonic are available (532 and 355 nm wavelength). The pulse duration is selectable from 35 ps to 500 ps. For

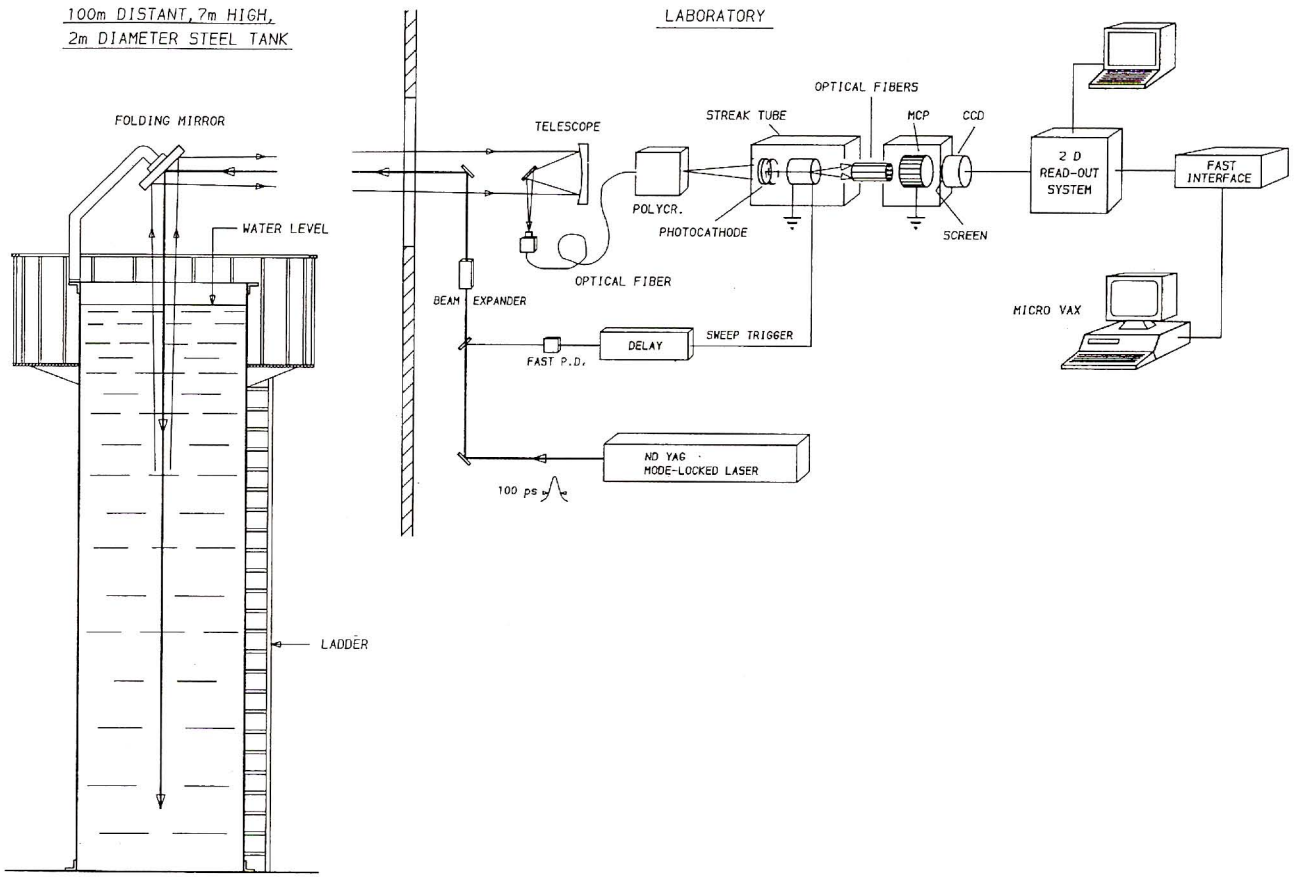

Fig. 1 - Laboratory experimental setup for remote measurements on an artificial water column.

remote measurements on the water column, we typically use a 100 ps pulse with an energy ofabout 20 mJ at 355 nm. The beam is sent through a beam expander in order to minimize the spot diameter on the target (typically 6 cm in diameter on the water surface).

The artificial water column is a 7 m high, 2 m in diameter steel tank standing at 100 m from the laboratory; a folding mirror on top serves to deviate the laser beam into the water column.

The receiving telescope is of Newtonian design with a 25 cm in diameter primary mirror and 85 cm focal length. At the focal point, the light is collected with an optical fiber and brought to the detector input.

The detector is a streak camera (Hadland Photonics Imacon 500) coupled to a polychromator in order to obtain fully spectro-temporal measurements. A measurement results in a 576 x 385 pixels CCD image in which the signal is temporally dispersed along the x axis and spectrally along the y axis; the signal intensity at each pixel is coded on 12 bits. The spectral dispersion used for the measurements presented in this paper yield a spectral range from 340 to 710 nm. The measurement time window is selectable on the streak camera; it was here 42 ns. When using a 0.40mm fiber, the spectral resolution is found to be 15 nm (FWHM); when using a 0.1 mm fiber it is measured to be limited to 7 nm (FWHM) by the polychromator itself. The temporal resolution is determined by the convolution ofthe laser pulse duration with the time equivalent to the fiber image diameter on the streak tube photocathode. The gain of the system can be varied by acting on the high voltage applied on the MCP image intensifier interposed between the streak tube output phosphor and the CCD.

A streak camera needs to be triggered some tens of nanoseconds before the arrival of the signal. The triggering pulse is generated by splitting part of the beam at the laser output to a fast photodiode. This pulse is then appropriately delayed to anticipate the signal by the exact required time. In remote measurements, the signal delay is provided by the time of flight from the laser to the target and from the target to the telescope (670 ns for a target at 100 m).

When performing measurements on samples in the laboratory, the necessary delay is obtained by making the laser pulse travel about 26 m before it is focalized on the

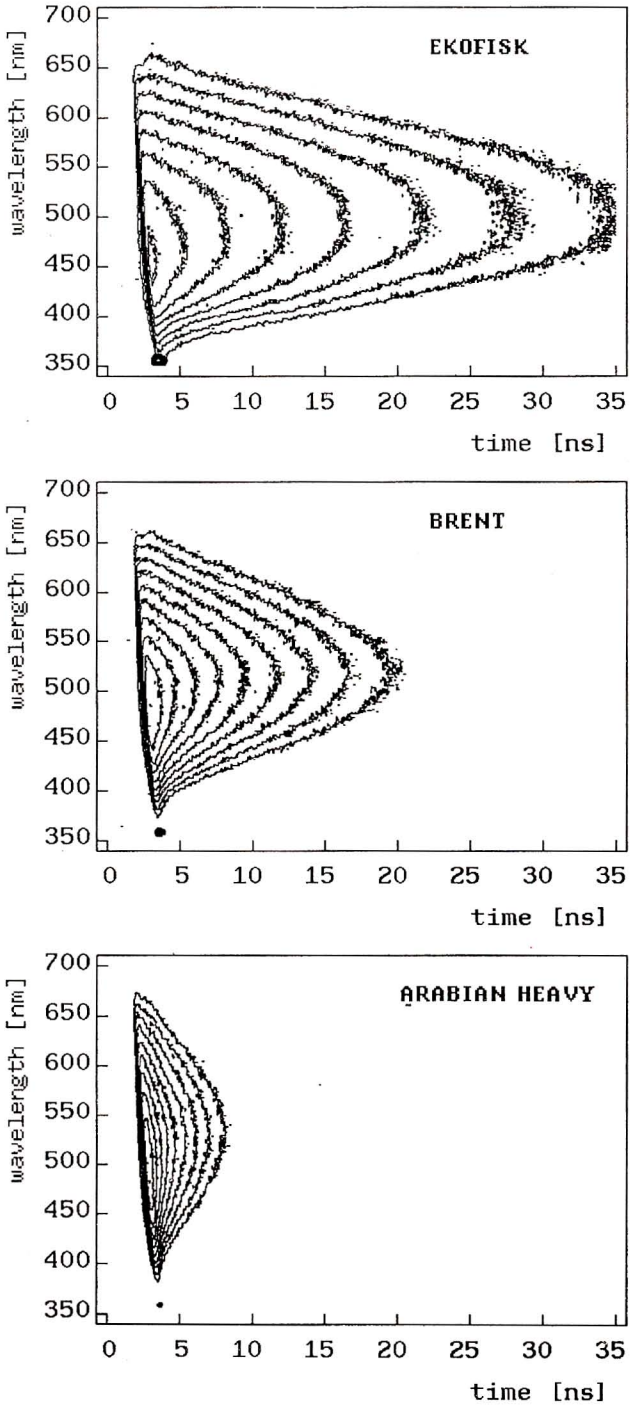

Fig. 2 - Fluorescence spectro-temporal images obtained with the streak camera system on three crude oils: Ekofisk (density 0.804 g/ml), Brent (0.834 g/ml) and Arabian heavy (0.887 g/ml). The representation is logarithmic (the "distance" between two curves corresponds to a constant factor in the signal intensity).

sample. In this case the fluorescence light is usually collected by simply positioning the optical fiber close to the illuminated spot on the sample.

2. LABORATORY RESULTS ON CRUDE OILS

Figure 2 shows the fluorescence spectro-temporal images obtained by exciting three crude oils at 355 nm: Ekofisk (density: 0.804 g/ml), Brent (0.834 g/ml) and Arabian heavy (0.887 g/ml). These measurements were performed in the laboratory with an optimal signal statistics (the images are the result of 6,000 laser shots) and with a high temporal resolution (0.5 ns FWHM). The 0.1 mm fiber was used giving a 7 nm spectral resolution (FWHM).

Figure 3 shows the detailed time decay in three 20 nm wide spectral bands of the Kirkuk fluorescence (density 0.848 g/ml).

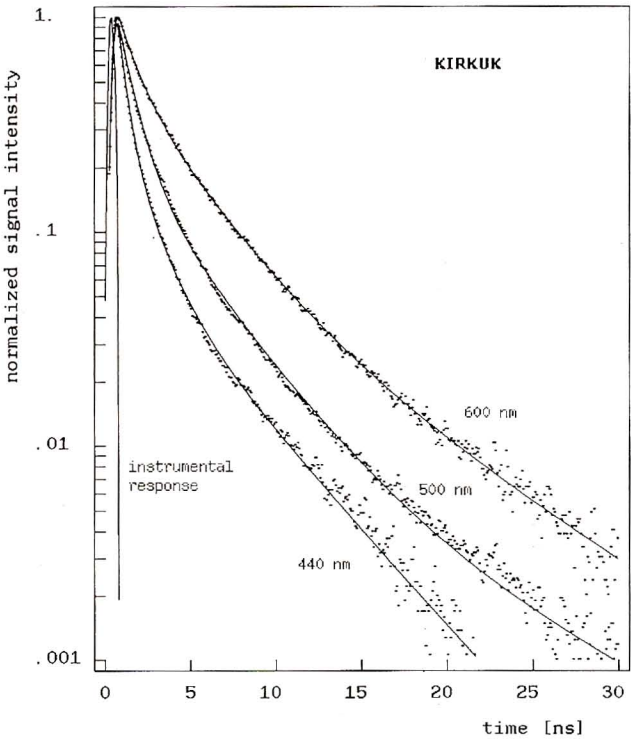

Fig. 3 - Fluorescence time decay of Kirkuk crude oil in three, 20 nm wide, spectral bands. The solid curves represent the fitting with a linear combination of three exponential functions. The following decay times (and relative initial amplitudes) were found: 440 nm: 0.46 ns (0.76), 1.44 ns (0.20) and 4.59 ns (0.06) 550 nm: 0.86 ns (0.80), 3.47 ns (0.19) and 9.82 ns (0.01) 600 nm: 1.00 ns (0.52), 3.31 ns (0.41) and 8.23 ns (0.07).

The solid curves represent fittings on the basis of a linear combination of exponential functions. The time decay in the long wavelength bands of the lighter oils is well described by two exponential components but we generally needed to use a minimum of three components, that is one more than is reported in other studies (Rayner and Szabo,1978; Camagni et a1.,1988). The reason is probably the high temporal resolution of these measurements which

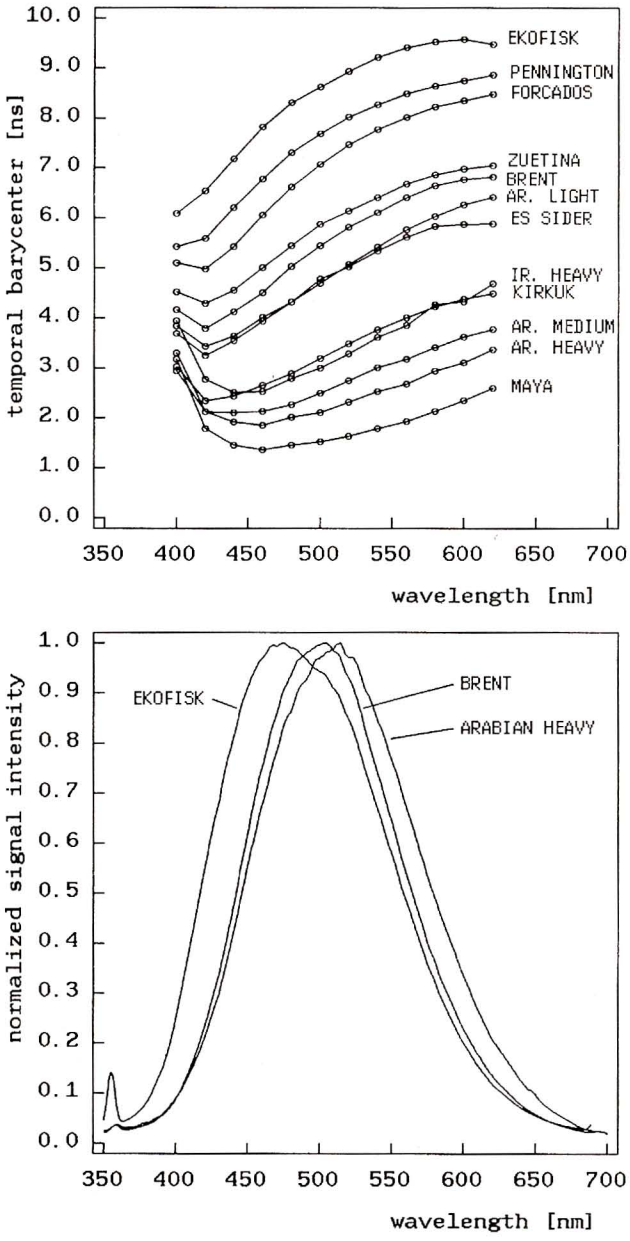

Fig. 4 - Fluorescence temporal barycenter calculated in 20 nm wide spectral bands for 12 crude oils (top) and three typical time - integrated fluorescence spectra (not corrected for the instrumental response). The measurements were performed on bulk samples.

reveal a fast component otherwise buried in the instrumental response. The exponential time decays found in the analysis of the twelve measured crude oils range from 0.4 to 18 ns. It should be emphasized that,at this stage, the multi-exponential analysis is only a way mathematically describing the decay ; to our knowledge, a model linking these time constants to the chemical and physical properties of the oil does not exist. Besides, this kind of analysis can only be performed on high quality data, difficult to obtain in field conditions. Therefore, a practical identification criterion must be based on other parameters which may be even more empirical but which can be determined with a higher reliability. A proposal is to base the identification on the time integrated fluorescence emission spectrum and on the signal temporal barycenter measured in several spectral bands. Such curves, retrieved from the laboratory series of measurements are represented in figure 4.

They confirm the general features of the crude oils fluorescence already found in other studies:

- the fluorescence decay is wavelength dependent: it is generally faster at shorter emission wavelengths. This trend is observed for all the measured oils, though a minimum in the temporal barycenter progressively appears with increasing oil density.

- the wavelength of maximum emission moves towards the longer wavelengths br heavier oils.

- from the point of view of their fluorescence, the crude oils can be classified in three groups; this is particularly evident from the temporal barycenter curves.

The weathering effects on the oils fluorescence cannot be ignored but contradictory results are reported on this subject. We will briefly present here a recent experiment concerning the evaporation. A film of a light crude oil (Pennington) was deposited on sea water and its fluorescence as a function of time was measured with the method described above. The film thickness is not known; it was visually semi-transparent and of a yellowish colour. As, on the contrary, it was optically dense to the exciting pulse at 355 nm, its thickness was no less than a few microns. The temporal barycenter curve and emission spectrum measured immdiately after the deposition and after various lapses of time are shown in immediately after the deposition and after various lapses of time are shown in figure 5.

It can be seen that the changes in the fluorescence characteristics are logical with the general trends observed on different oils: as the light fractions disappear, the time decay fastens and the emission maximum shifts to longer wavelengths. After 42 hours the changes are still modest but sufficient to induce an error in the detailed identification. However, the oil would still be classified in the light group; such a group classification is, we think, the realistic

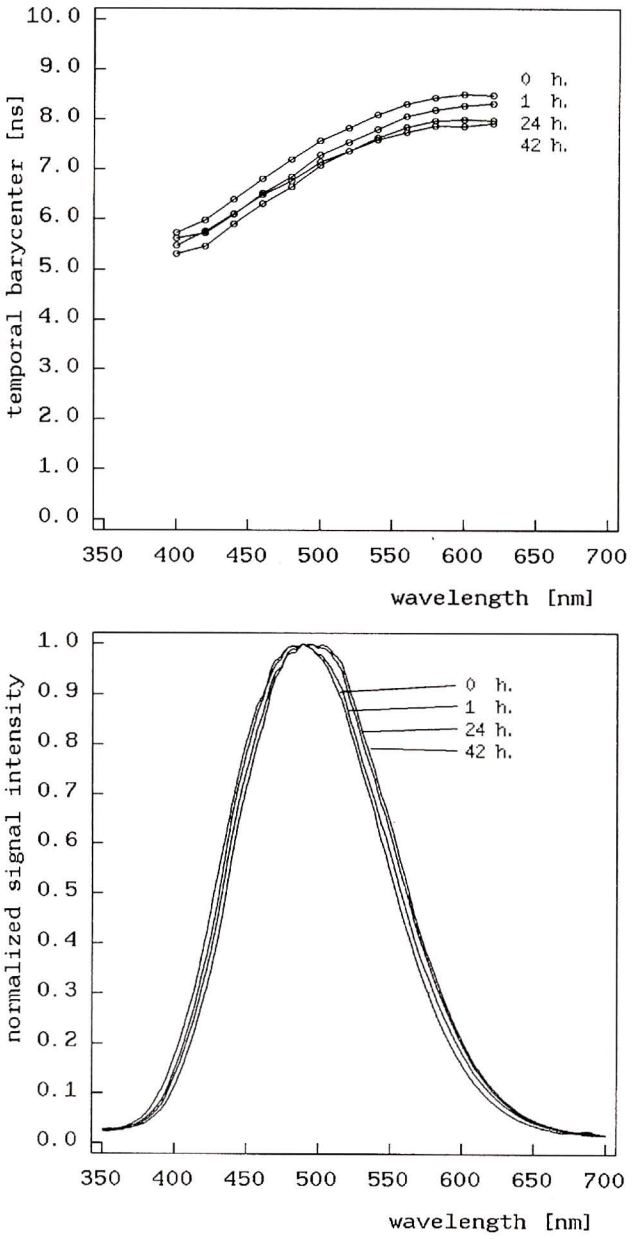

Fig. 5 - Fluorescence characteristics of a Pennington crude oil film deposited on sea water as a function of time (room temperature, no wind).

objective of remote oil fingerprinting. We also performed a measurement on a freshly made mousse of Pennington and found negligible differences with respect to the film response.

Our intention is to conduct more systematic investigations on the weathering efects and on the problem of the superimposition of the sea water DOM fluorescence on the oil signal. This last subject will be studied by using the artificial water column which allows us to have a realistic depth of water under the oil film.

3. LABORATORY RESULTS ON THE WATER COLUMN

We will briefly report here an experiment on the water column which was intended to assess the possibilities of the time-resolved measurements for the analysis of waters containing various concentrations of DOM. More details on such experiments can be found elsewhere (Bertolini et al., 1991; Verdebout and Koechler, 1991).

The potential of time resolution for the water column analysis lies in the fact that it gives access to the depth dependence ,of the various signals. We used a simple model which neglects the multiple scattering and assumes a uniform water column; in this case, one can write for the time dependent signals:

backscattering

$$s_b(t) = \frac{T^2 \cdot No \cdot \Omega o \cdot \beta_b(180) \cdot c'}{2 \cdot \left(1 + \frac{c' \cdot t}{2 \cdot Ho}\right)} \cdot \exp(-k_e \cdot c' \cdot t) \quad (1)$$

Raman diffusion

$$s_R(t) = \frac{T^2 \cdot No \cdot \Omega o \cdot \beta_R(180) \cdot c'}{2 \cdot \left(1 + \frac{c' \cdot t}{2 \cdot Ho}\right)} \cdot \exp\left(-\frac{k_e + k_R}{2} \cdot c' \cdot t\right) \quad (2)$$

DOM fluorescence observed at wavelength λ

$$s_f(t) = T^2 \cdot No \cdot \Omega o \cdot \beta_f(180) \cdot \Sigma_i \frac{\alpha_i}{\tau_i} \exp\left(-\frac{t}{\tau_i}\right) \cdot \int_0^{\frac{c' t}{2}} \frac{\exp\left[-\left(k_e + k_\lambda - \frac{2}{c' \tau_i}\right) \cdot h\right]}{\left(1 + \frac{h}{H o}\right)^2} \cdot dh \quad (3)$$

where

N_o	is the number of photons in the exciting pulse
T	is the transmission coefficient of the air/water interface (considered wavelength independent)
Ω_o	is the collection solid angle from the water surface
H_o	is the distance between the telescope and the water surface
c'	is the speed of light in water (considered wavelength independent)
t	is the time counted from the instant of arrival of the surface signal

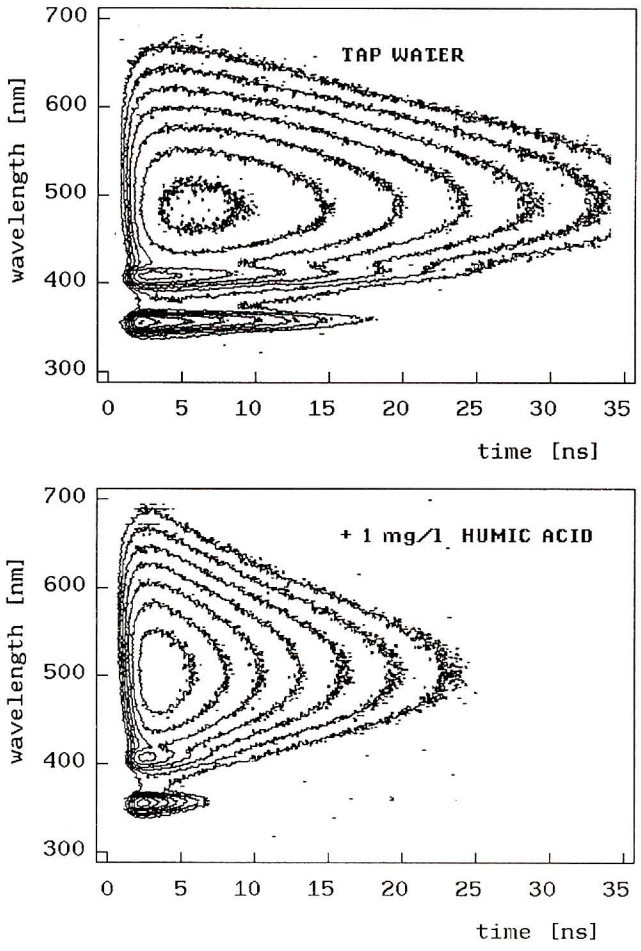

Fig. 6 - Spectro-temporal imags obtained from the artificial water column with 355 nm excitation. The tank was initially filled with tap water (top); humic acid was then added to obtain a maximum concentration of 1mg/l (bottom).

k_e, k_R, $k\lambda$ are the water beam attenuation coefficients at the excitation,Raman emission and observed DOM fluorescence wavelengths respectively

$\beta_b(180)$ is the volume scattering function at the back-scattering angle

$\beta_R(180)$ is the volume Raman diffuion function at 180 degrees

β_f is the volume fluorescence emission function at 180 degrees

a_is, τ_is are the parameters describing the DOM fluorescence intrinsic decay at the observed wavelength as a linear combination of exponentials according to

$$\Sigma_i \frac{a_i}{\tau_i} \exp\left(-\frac{t}{\tau_i}\right) \quad with \quad \Sigma_i \alpha_i = 1$$

The experiment consisted in filling the tank with tap water and then in adding known quantities of an industrial humic acid (FLUKA 53680) to simulate an increasing concentration of DOM. Humic acid is a complex organic acid resulting from the degradation of vegetal materials. The measurements were performed using a 0.4 mm fiber and a 100 ps laser pulse at 355 nm, the spectral and temporal resolutions were 15 nm and 1.2 ns respectively (FWHM); the signal was accumulated on 6,000 laser shots. Figure 6 shows the spectro-temporal images obtained with the initial water and with 1 mg/l of humic acid.

Figure 7 shows the uncorrected time integrated spectra and figure 8 the temporal shape of the backscattering, Raman and DOM fluorescence (at 500 nm) signals for the initial water; in this last figure, the solid curves represent the fitting based on expressions (1) to (3) further convoluted with the instrumental response.

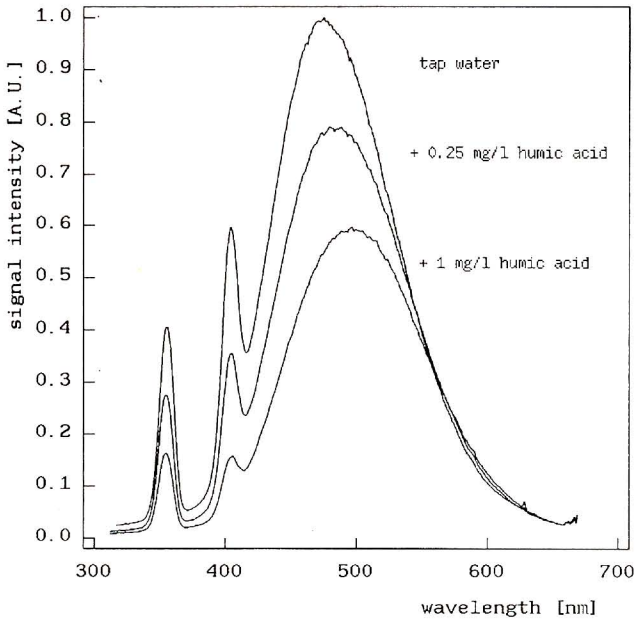

Fig. 7 - Uncorrected time integrated spectra for tap water and two humic acid concentrations. The backscattering peak is at 355 nm, the water Raman line at 404 nm.

To reproduce the backscattering signal, it was necessary to add an instantaneous response at time 0 to take into account tbe scattering by the water surface. As the Raman is superimposed on a snlall fluorescence signal, the time dependence in the corresponding spectral band was fitted as a weighted sum of expressions (2) and (3), the weights being determined by interpolating the time integrated spectrum. To fit the fluorescence signal, it was necessary

to use three exponential components for the intrinsic fluorescence decay. It should be noticed that the DOM fluorescence signal shows a build up time not present in an oil film signal; this provides a clue to distinguish the two cases.

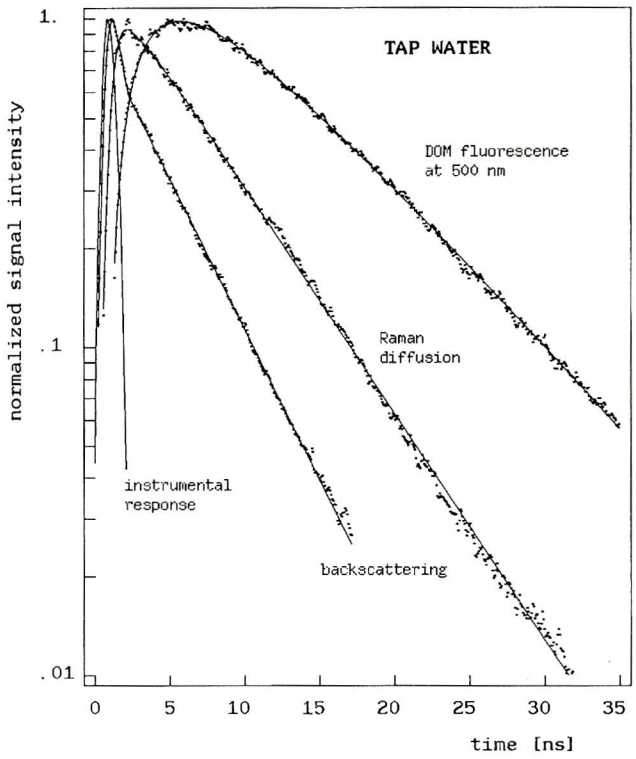

Fig. 8 - Time dependence of the backscattering, Raman diffusion and DOM fluorescence (at 500 nm) signals for tap water. The solid curves represent the fitting based on the model described in the text.

Table I reports the values for the attenuation coefficient retrieved, by the fitting procedure, from the lidar signals and measured on samples of water with a spectrophotometer.

humic acid			wavelength [nm] 355	404	440	500	560
0.		SP	0.92	0.42	0.23	0.16	0.08
		L	0.88	0.44	0.26	0.12	0.06
0.25	mg/l	SP	1.51	0.56	0.49	0.14	0.12
		L	1.57	0.54	--	--	--
0.5	mg/l	SP	2.27	0.89	0.73	0.35	0.27
		L	2.38	0.84	--	--	--
0.75	mg/l	SP	2.93	1.32	0.81	0.48	0.24
		L	2.81	1.34	--	--	--
1.0	mg/l	SP	3.98	2.31	1.44	0.94	0.62
		L	3.42	2.46	--	--	--

Table I: Values of the attenuation coefficient (in m-1) for the various concentrations of humic acid as measured with the spectrophotometer (SP) and as recovered from the LIDAR signals (L).

The agreement is satisfactory in the case of the backscattering and Raman wavelengths except for the highest concentration of humic acid; this is probably due to the increasing influence of the multiple scattering which is governed by the value of the product of the attenuation coefficient by the spot radius on the surface (Gordon,1982). In the case of the DOM fluorescence signals, reasonable values for k could be obtained from the lidar signals only for the water without added humic acid. For higher attenuation coefficients, the fitting procedure, though providing an accurate reproduction of the signal, yielded unrealistic values for the parameters. It seems that the fitting is successful in retrieving the attenuation coefficient only if the associated time constant is longer than the time constants of the intrinsic fluorescence decay (the signal temporal dependence at long times is then determined by the attenuation coefficient).

Figure 9 shows the time-integrated backscattering and DOM fluorescence signals as a function of the humic acid concentration, once corrected for the attenuation coefficient (using the spectrophotometer values).

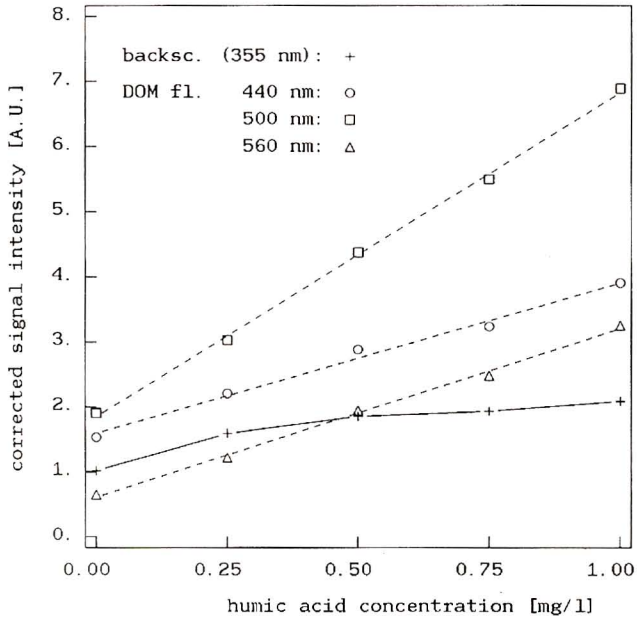

Fig. 9 - Corrected intensity of the time integrated signal at the backscattering wavelen@dh and in three spectral bands of the DOM fluorescence, versus the humic acid concentration.

In this experiment, the backscattering coefficient should be only weakly affected by the additional humic acid; the slight increase in the corrected signal intensity is probably due to the recirculation of the water performed after each addition of humic acid. This operation is likely to have put in suspension particles initially deposited on the bottom

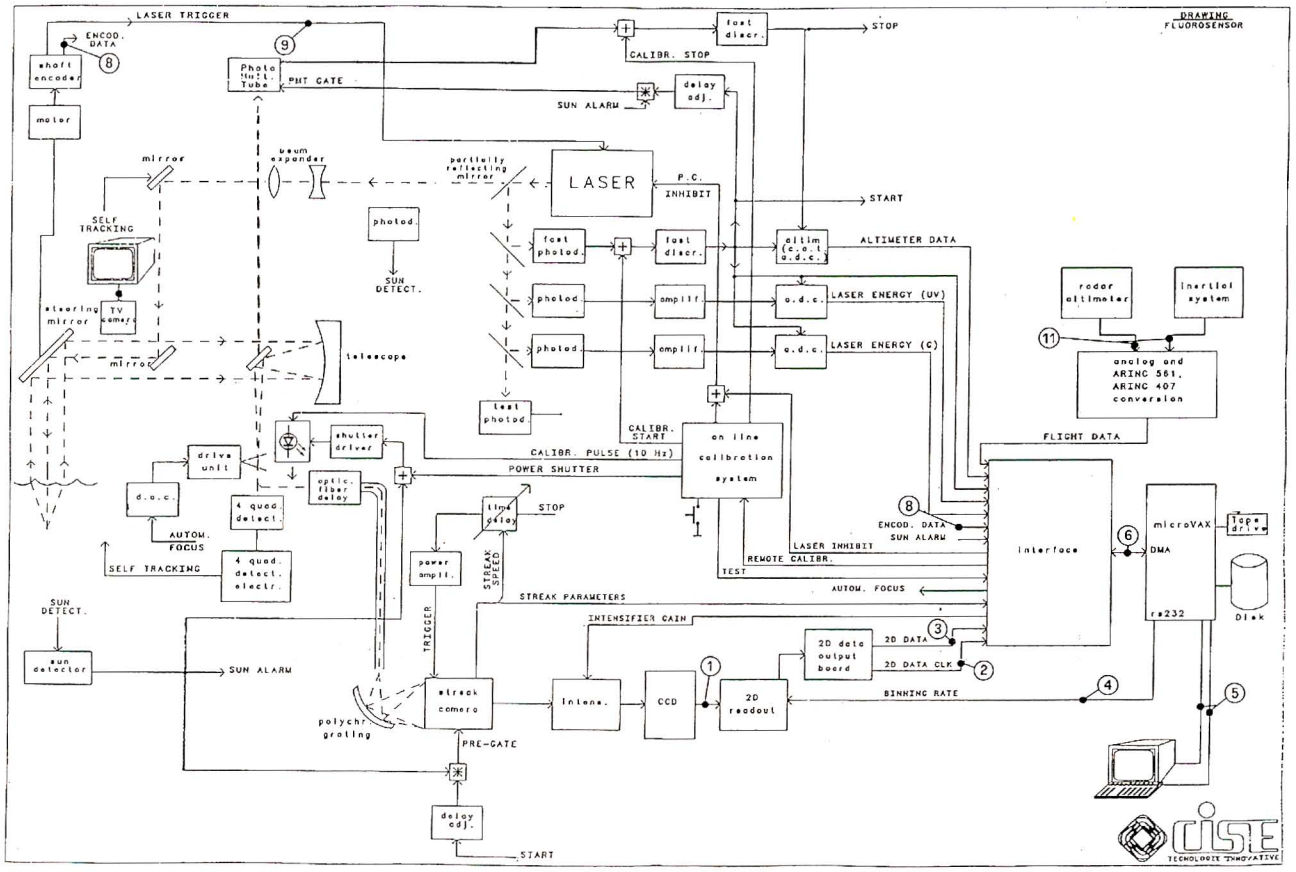

Fig. 10 - Block diagram of the "Time Resolved Lidar Fluorosensor".

of the tank. The corrected DOM fluorescence signals show the expected linear dependence at the three selected wavelengths.

This experiment is a first assessment of the possibility of measuring the water attenuation coefficient from high resoluiion time-resolved lidar signals. Using our simulation facility, we intend to conduct further studies by varying the scattering coefficient and on the detection of chlorophyll fluorescence. It also remains to check how the waves will affect the signals temporal dependence, though this effect should be minimized by the small spot diameter (Rayner et a1., 1978; Gehlhaar, 1982).

4. THE FLIGHT INSTRUMENT

The "Time Resolved Lidar Fluorosensor" is the instrument designed to perform the type of measurements described above from an aerial platform. It was built for the JRC by the CISE spa of Milan. Its architecture is basically that of the laboratory setup (see figure 10).

The source is an actively mode-locked Nd-YAG laser using a SFUR cavity (Self Filtering Unstable Resonator) which makes it particularly compact. It delivers maximum energies of 30 mJ at 355 nm and 60 mJ at 532 nm. The pulse duration was measured to be slightly longer than 1 ns (FWHM). The beam is sent towards the target along the axis of the receiving telescope after passing through a beam expander which serves to minimize the spot diameter on the sea surface. The output beam has a 2 cm diameter and a 0.15 mrad divergence so that the spot diameter is approximately 5 cm in diameter at 100 m. The maximum firing rate is 10 Hz.

The detector is a streak camera identical to the laboratory one. The polychromator is fitted with two gratings allowing to choose between three spectral ranges: 340 to 710 nm with a resolution of 15 nm, 340 to 580 nm or 520 to 760 nm with a resolution of 10 nm. The Newtonian telescope is 30 cm in diameter with a focal length of 85 cm. The signal light is collected by a 20 m long, 0.4 mm in diameter optical fiber and brought to the polychromator input. The optical liber diameter determines the receiver field of view which is 0.5 mrad.

With such a narrow beam/narrow field of view geometry, the alignment of the system becomes critical. Therefore, it has been fitted with an auto-alignment feedback loop acting on one of the mirrors in the beam path; the error signal is generated by a four quadrant detector looking at a fraction of the output beam. It has been checked that this feedback mechanism succeeds in maintaining the pointing stability within 0.2 mrad.

Another problem was the generation of the trigger pulse for the streak camera; this can no longer be done at the laser output as the variability of the distance from the aircraft to the sea surface would introduce a jitter destroying the time resolution. The triggering pulse is therefore generated, by a photomultiplier, from the return signal itself. The light falling in the shadow of the telescope secondary mirror is used for this purpose. The necessary delay between the trigger pulse and the arrival of the signal on the streak camera is provided by the optical fiber.

The system contains two computers: the "2D readout system" dedicated to the control of the streak camera detector and a micro VAX II/GPX as the main computer. This last one controls in particular the automatic positioning of the optical fiber at the telescope focus as a function of the target distance, according to a predetermined law. The distance is calculated from the time delay between the laser pulse emission and the arrival of the signal.

The instrument is also fitted with laser energy monitoring detectors, a built-in rough calibration system and a protection system against excessive solar illumination.

In order to use the 10 Hz firing rate of the laser and still acquiring the single shot measurements, it was necessary to reduce the amount of data generated by the CCD (a full resolution image represents 0.5 Mb). Such a possibility is provided by the 2D system which allows to programm macro-pixels at the readout time ("binning"). The maximum data acquisition rate with storage on the VAX hard disk is 30 kwords, implying the reduction of each image size to 3,000 pixels. This does not exclude to use the system with a higher CCD image resolution but a lower acquisition rate. The choice can also be made to accumulate, on the CCD, the signal produced by a large number of laser shots in order to obtain a better statistics. The present capacity of the hard disk is 70 Mb.

The system provides a real time display to the operator. This display, for reasons of limited data throughput, is restricted to the spectrum at a selectable time, 5 time traces at selectable wavelengths, indication of the laser energy, target distance, receiver parameters and flight data.

The instrument is housed in five containers, it weights 520 kg and has a power consumption of 3.1 kW partitioned between 28 V DC and 115 V AC (400 Hz) (see figure 11).

Fig. 11 - View of the TRLF, the four containers in the foreground contain the VAX computer (top left), the VAX monitor (top right), the laser power supply (bottom left) and the streak camera computer (bottom right). The larger container in the background contains the optical system.

The system has been tested on the ground with both oils and water column targets. Figure 12 shows the result of a single laser shot on a bulk sample of Brent crude oil placed at 200 m.

The statistics is of course poorer than that of the laboratory measurements but sufficient, to implement the simple identification criterion defined above. Figure 13 shows a measurement performed on a lake by operating the instrument from a motorvan on the bank. The distance to the water surface was about 100 m and the image was summed on 200 laser shots.

We are now collaborating with the society AGUSTA to test the instrument from an helicopter. The helicopter offers a greater flexibility with respect to an airplane as it can fly very low, at low speed and can hover in order to allow a high quality measurement by accumulation without loosing in spatial resolution. We recently performed the first test flight on an AGUSTA AB412 helicopter which demonstrated the mechanical and electromagnetic compatibility between the instrument and the aircraft.

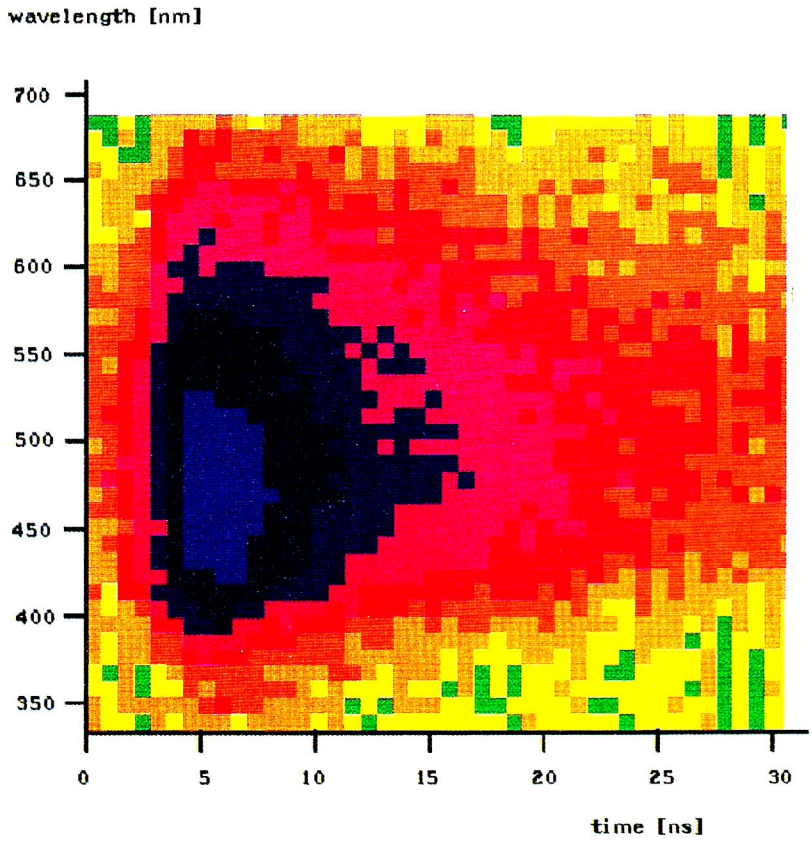

Fig. 12 - Spectro-temporal fluorescence image of Brent crude oil obtained with a single laser pulse at a distance of 200 m. The 10 x 10 pixels binning allows to acquire such measurements at 10 Hz.

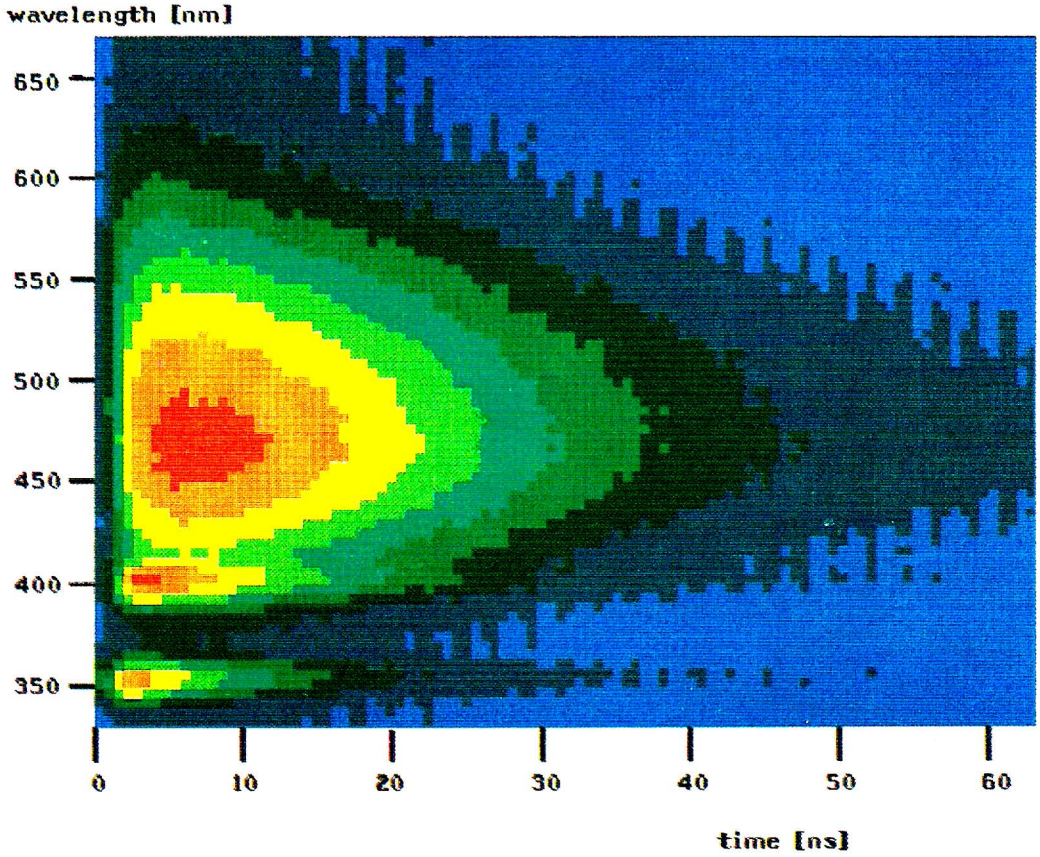

Fig. 13 - Spectro-temporal image: obtained on the lago Maggiore; the binning is here 5 x 5 pixels. The measurement was performed with 200 laser pulses and at a distance of 100 m.

CONCLUSIONS

Laboratory simulation experiments have demonstrated the potentialities of high temporal resolution for the remote characterization of crude oils and to measure the water attenuation coefficient. More work is however needed on the efects of the weathering processes and on the problem of distinguishing oil fluorescence against the background of the DOM signal. Similarly, the simulations on the water column have to be pursued to enlarge the laboratory experimental basis and cover a wider range of natural situations (variable scattering, chlorophyll fluorescence). Another indispensable study is the simulation of the sea surface structure effects on the signals time dependence.

The flight instrument designed to perform this type of measurements in field has shown promising results when tested on the ground. The evaluation of its performances from an helicopter is now under way.

ACKNOWLEDGMENTS

The authors are indebted to Dr. P. Tittarelli of the "Stazione Sperimentale dei Combustibili (San Donato Milanese, Italy) for the supply of all crude samples.

Thanks are due to Messrs. R. Van Wijk, E. Ghezzi and M. Morelli for their efficient technical support, Mr. G.M. Ferrari for having performed the spectrophotometer measurements and Mrs. M.R. Graglia for the secretary assistance. The help of Mr. A.Pegoraro for the technical drawings and mechanical design is gratefully acknowledged.

REFERENCES

Barbini R., Fantoni R., Palucci ,a., Ribezzo S. and Van Der Steen, 1990, Fluorosensore laser (XeCl) per misure sul territorio risolte spettralmente e temporalmente, atti 1o Convegno Nazionale Strumentazione e Metodi di Misura Ottici", Milano Segrate, Italy, pp. 381-385.

Bertolini G., Koechler C. and Verdebout J., 1991, The use of a time-resolved lidar to study the water column, in the proceedings of the "Fifth International Colloquium on the Physical Measurements and Signatures in Remote Sensing", Courchevel, France, 14th-18th January 1991.

Bristow M., Nielsen D., Bundy D. and Furtek R., 1981, Use of water Raman emission to correct airborne laser fluorosensor data for effects of water optical attenuation, Applied Optics, Vol. 20, No. 17, pp. 2889-2906.

Burlamacchi P., Cecchi G., Mazzinghi P. and Pantani L., 1983, Performance evaluation of UV sources for lidar fluorosensing of oil films, Applied Optics, Vol. 22, No. 1, pp. 48-53.

Camagni P., Colombo G., Koechler C., Omenetto N., Pedrini A. and Rossi G., 1988, Remote characterization of mineral oils by laser fluorosensing: basic diagnostics and simulation experiments, Commission of the European Communities,Ispra Establishment (Varese, Italy), EUR 11781 EN.

Diebel-Langohr D., Hengstermann T., Reuter R., Cecchi G. and Pantani L., 1985, Measuring oil at sea by means of an airborne laser fluorosensor, in "The Archimedes 1 Experiment", pp. 123-142, R.H. Gillot and F. Toselli Eds., Commission of the European Communities, Ispra Establishment, EUR 10216 EN, 223 p.

Diebel D., Hengstermann T. and Reuter R., 1987, Classification of oil types with time-resolved fluorescence signal detection: a computer model study, in "Remote Sensing of Pollution of the Sea", pp. 266-280, R.Reuter and R.H. Gillot Eds., Conmmission of the European Communities, Ispra Establishment Varese,Italy) and BIS University of Oldenburg (Germany), S.P.I.87.46.

Dittmann R.d. and Ross Hallett F., 1988, Remote sensing of phytoplankton by laser fluorosensor: effect of self attenuation, Applied Optics, Vol. 27, No.15, pp. 3290-4.

Dudelzak A., Babichenko S.m., Poryvkina L.v. and Saar K.J., 1991, Total luminescent spectroscopy for remote laser diagnostics of natural water conditions, Applied Optics, Vol. 30, No. 4, pp. 453-8.

Exton R.J., Houghton W.M., Esaias W., Harris R.C., Farmer F.H. and White H.H., 1983, Laboratory analysis of techniques for remote sensing of estuarine parameters using laser excitation, Applied Optics, Vol. 22, pp.54-64.

Gehlhaar U., 1982, Computer simulations and theory of oceanographic fluorescence lidar signals: effects of sea surface structure, Applied Optics, Vol. 21, No. 20, pp. 3743-55.

Gordon H.R., 1982, Interpretation of Airborne oceanic lidar: effects of multiple scattering, Applied Optics, Vol. 21, No. 16, pp. 2996-3001.

Hengstermann T. and Reuter R., 1990, Lidar fluorosensing of mineral oil spills on the sea surface, Applied Optics, Vol. 29, No. 22, pp. 3218-27.

Hoge F.E., 1983, Oil film thickness using airborne laser-induced oil fluorescence backscatter, Applied Optics, Vol. 22, No. 21, pp. 3316-18.

O'neil R.A., Buja-Bijunas L. and Rayner D.M., 1980, Field performance of a laser fluorosensor for the detection of oil spills, Applied Optics, Vol. 19,No. 6, pp.863-70.

Poole L.R. and Esaias W.E., 1983, Influence of suspended inorganic sediment airborne laser fluorosensor measurements, Applied Optics, V01.22, No. 3, pp. 380-1.

Rayner D.M., Lee M. and Szabo A.G. 1978, Efect of sea state on the performance of laser fluorosensors, Applied Optics, Vol. 17, No. 17, pp. 2730-33.

Rayner D.M. and Szabo A.G., 1978, Time-resolved laser fluorosensors laboratory study of their potential in the remote characterization of oil, Applied Optics, Vol. 17, No. 10, pp. 1624-30.

Verdebout J. and Koechler C., 1991, Time-resolved lidar measurement on an artificial column, to be published in the proceeding of the "1991 International Geoscience And Remote Sensing Symposium", Espoo, Finland, June 3-6, 1991.

Visser H., 1979, Teledetection of the thickness of oil films on polluted water based on the oil fluorescence properties, Applied Optics, Vol. 18, No. 11, pp. 1746- 49.